Realizing Visible Light Excitation of Tb^{3+} via Highly Efficient Energy Transfer from Ce^{3+} for LED-Based Applications

Wenge Xiao, Xiaofeng Liu, Jiahua Zhang,* and Jianrong Qiu*

Trivalent terbium (Tb^{3+})-activated luminescence materials usually show highly efficient green emission with the full width at half maximum of merely 10 nm, but suffer from the unsatisfactory excitable wavelength (<380 nm) as well as the inefficient light absorption. Here, the realization of efficient visible light excitation of Tb^{3+} is demonstrated in terbium-concentrated garnet Ca$_2$TbHf$_2$Al$_3$O$_{12}$ (CTHA) by introducing Ce^{3+} as the sensitizer. Owing to highly efficient energy transfer from Ce^{3+} to Tb^{3+}, CTHA:Ce^{3+} combines advantages of the extra narrow green emission of Tb^{3+} peaking at 544 nm and the efficient broad excitation of Ce^{3+} covering the short-wavelength visible light from 380 to 450 nm. The color gamut of the prototype white light-emitting diode (LED) by using CTHA:Ce^{3+} as the green emitter can reach 95% (coverage ratio) of National Television Standards Committee (NTSC) space in Commission Internationale de L'Eclairage (CIE) 1931, indicating its great potential for LED (or laser diode)-based applications.

Lanthanide-doped luminescence materials have been intensively studied due to their broad applications ranging from lightings, lasers, photovoltaics, to biological imaging and therapies.[1] Intra-configurational 4f→4f transitions of trivalent lanthanide ions (Ln^{3+}) endow them with abundant emission colors, sharp emission peaks, and long lifetimes, which, however, make them suffer from very low absorption of the excitation light due to the 4f→4f parity-forbidden transitions.[2] Among these Ln^{3+} ions, Tb^{3+} is the most efficient activator with predominant narrow-band green emission around 544 nm originating from the $^5D_4$→$^7F_5$ transition. Because of the large energy gap (about 15 000 cm^{-1}) between the emitting level

Dr. W. Xiao, Prof. J. Qiu
State Key Lab of Modern Optical Instrumentation
College of Optical Science and Engineering
Zhejiang University
Hangzhou 310027, P. R. China
E-mail: qjr@zju.edu.cn
Prof. X. Liu
School of Materials Science and Engineering
Zhejiang University
Hangzhou 310027, P. R. China
Prof. J. Zhang
State Key Laboratory of Luminescence and Applications
Changchun Institute of Optics, Fine Mechanics and Physics
Chinese Academy of Sciences
Changchun 130033, P. R. China
E-mail: zhangjh@ciomp.ac.cn

The ORCID identification number(s) for the author(s) of this article can be found under https://doi.org/10.1002/adom.201801677.

$^5D_4$ and its next lower level $^7F_1$, the multiphonon relaxation of Tb^{3+} is usually negligible and not so susceptible to the maximum phonon energy as other Ln^{3+} ions like Er^{3+}, Ho^{3+}, and Tm^{3+}; therefore, Tb^{3+} shows intense green emission in most of the host materials including inorganic nanocrystals and lanthanide complexes, which have been researched for various applications, especially in lasers, lightings, and biological imaging.[3] Unfortunately, Tb^{3+} itself has no absorption band in the range from 380 to 480 nm, which largely restrict their practical applications, since the efficient and stable solid-state light sources (i.e., light-emitting diode (LED) or laser diode (LD)) for short-wavelength visible light (violet/blue: 400–460 nm) have been easily available and thus highly preferred.[4] Although the strategy of sensitization by Ce^{3+}, Eu^{2+}, and organic ligands has been extensively explored, the efficient excitation (or absorption) band of Tb^{3+} is still limited within the UV range (<400 nm).[5]

Several previous works have shown that the dominant energy transfer (ET) mechanism from Ce^{3+} (or Eu^{2+}) to Tb^{3+} is electric dipole–quadrupole interaction with the ET probability proportional to R^{-8}, where R is the distance from Ce^{3+} to Tb^{3+}, and thus ET process from Ce^{3+} to Tb^{3+} mainly occurs within the nearest Ce^{3+}–Tb^{3+} pairs.[6] Accordingly, large concentration (typically >20 mol%) of Tb^{3+} is required to achieve high ET efficiency (>95%) and thus obtain nearly pure Tb^{3+} emission. To accommodate sufficient quantity of Tb^{3+} without destabilizing or changing the original crystal structure, the host crystal should have lattice sites occupied by Ln^{3+} (mainly Lu^{3+}, Y^{3+}, Gd^{3+}, and La^{3+}), so that their ionic radii are similar and there is no need for charge compensation. For Eu^{2+}–Tb^{3+} codoped systems, however, those Ln^{3+} sites may also cause the coexistence of Eu^{3+} with Eu^{2+} even sintered under reducing atmosphere, which was confirmed to be luminescence killer for Eu^{2+} emission.[4c,7] As a result, high ET efficiency from Eu^{2+} to Tb^{3+} is usually accompanied by a substantial reduction of photoluminescence quantum efficiency (QE). By contrast, this problem does not exist in Ce^{3+}–Tb^{3+} codoped systems due to their same valence and similar ionic radii, and highly efficient Tb^{3+} emission sensitized by Ce^{3+} has been realized in several materials.[6,8] Nevertheless, Ce^{3+} has much shorter excitation band in wavelength as compared with Eu^{2+} given the same surroundings, and only a handful of Ce^{3+}-doped materials can be efficiently excited by violet/blue light.[9] Hence, efficient violet/blue light excitation of Tb^{3+}-activated materials has not yet been realized.

ADVANCED
SCIENCE NEWS
www.advancedsciencenews.com

ADVANCED
OPTICAL
MATERIALS
www.advopticalmat.de

It was reported that upon violet light excitation, Ce^{3+}-doped aluminate garnet $Ca_2LuHf_2Al_3O_{12}$ (CLHA) (CLHA:Ce^{3+}) exhibits efficient wideband cyan emission peaking at 484 nm,[10] which overlaps well with the excitation band of Tb^{3+} $^5D_4$ level, implying the possible existence of ET process from Ce^{3+} to Tb^{3+} if Tb^{3+} and Ce^{3+} are codoped. Furthermore, we found that only weak concentration quenching of Tb^{3+} emission happens in $Ca_2TbHf_2Al_3O_{12}$ (CTHA) where Tb^{3+} fully occupies the Lu^{3+} site in CLHA, which is beneficial and indispensable to achieving high ET efficiency from Ce^{3+} to Tb^{3+}. These two characteristics will allow us to obtain efficient pure Tb^{3+} emission under violet light excitation by introducing Ce^{3+} into CTHA. Herein, we demonstrate the realization of efficient violet/blue light (peaking at 410 nm) excitation of pure Tb^{3+} emission in CTHA:Ce^{3+} owing to high ET efficiency (approaching 100%) from Ce^{3+} to Tb^{3+}. CTHA:Ce^{3+} shows ultra-narrow-band green emission at 544 nm, good thermal stability as well as wide excitation band, indicating that it can be a potential narrow-band green phosphor for LED/LD-based applications.

The crystal structure of CTHA was examined by the powder X-ray diffraction (XRD) and confirmed by Rietveld refinement (**Figure 1**a). The crystallographic data and refinement parameters are summarized in Tables S1 and S2 in the Supporting Information. These results reveal that CTHA is one of the end members of the garnet-type $Ca_2Ln(Hf,Zr)_2Al_3O_{12}$ solid solutions with cubic structure, which is isostructural with the well-known crystals $Y_3Al_5O_{12}$ (YAG) and $Lu_3Al_5O_{12}$ (LuAG). The crystal structure of CTHA consists of a 3D network that each $[HfO_6]$ octahedron is connected to six $[AlO_4]$ tetrahedrons while each $[AlO_4]$ tetrahedron is connected to four $[HfO_6]$ octahedrons by sharing corners, and Ca^{2+}/Tb^{3+}/Ce^{3+} are arranged in the dodecahedral interstices of the network (Figure 1b). In addition, the lattice parameters ($a = b = c = 12.47$ Å, and $V = 1940.55$ Å^3) show an obvious increase compared with YAG ($a = b = c = 12.00$ Å, and $V = 1728.13$ Å^3) because the ionic radii of Ca^{2+} (1.12 Å) and Hf^{4+} (0.71 Å) are much larger than those of Y^{3+} (0.99 Å) and Al^{3+} (0.54 Å), respectively.[11]

The microstructure of CTHA was characterized by the high-resolution transmission electron microscopy (HRTEM). The
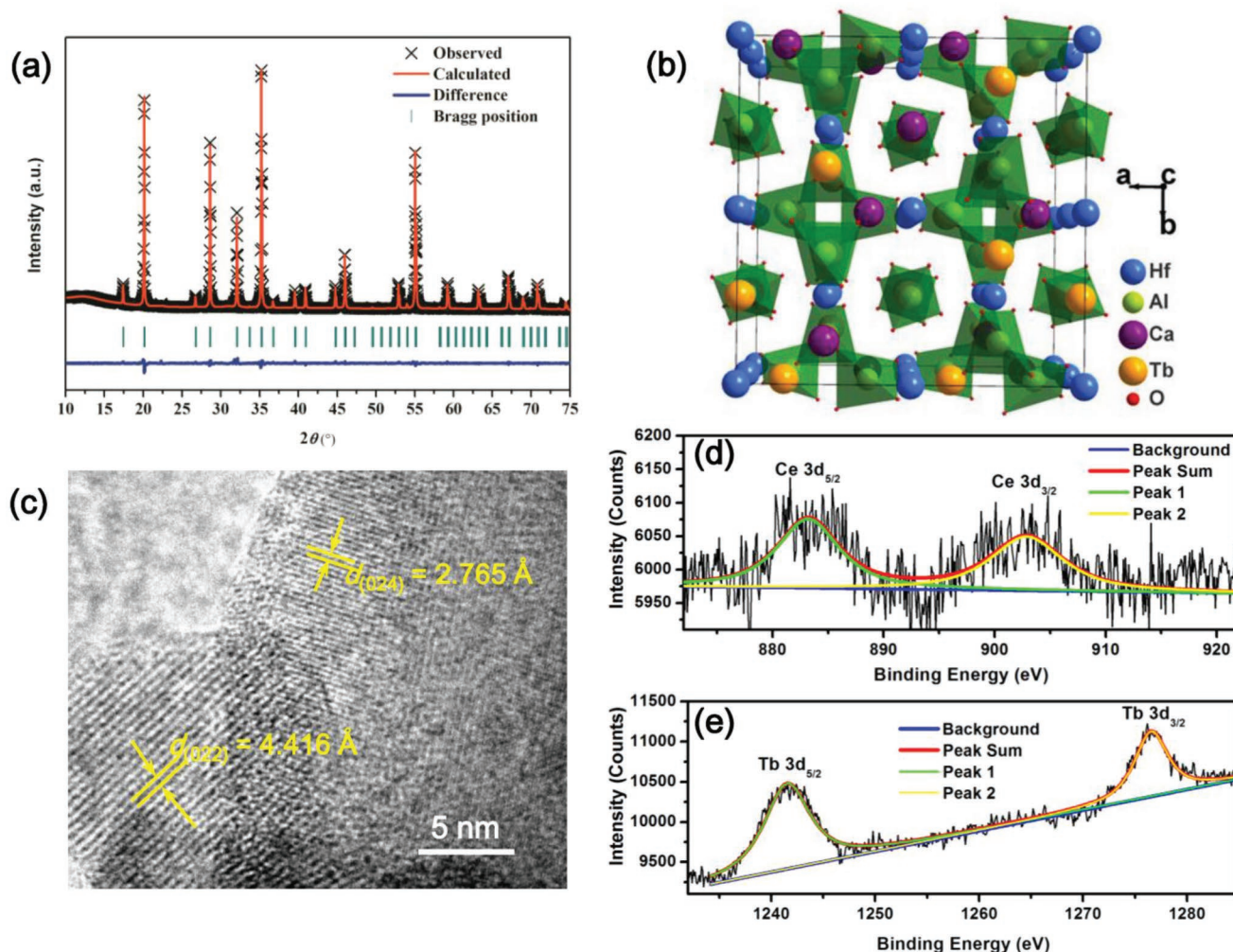

Figure 1. a) Rietveld refinement XRD pattern of CTHA. b) Crystal structure of CTHA. c) HRTEM images of CTHA. d) High-resolution XPS spectra of Ce (3d) and Tb (3d) of CTHA:0.05Ce^{3+}. Two distinct peaks at 883 (3d$_{5/2}$) and 903 eV (3d$_{3/2}$) are both attributed to Ce^{3+} and the Ce^{4+} related feature at 916.5 eV is absent. The two distinct peaks of Tb^{3+} (3d$_{3/2}$ and 3d$_{5/2}$) are located at 1277 and 1241 eV without additional peaks.
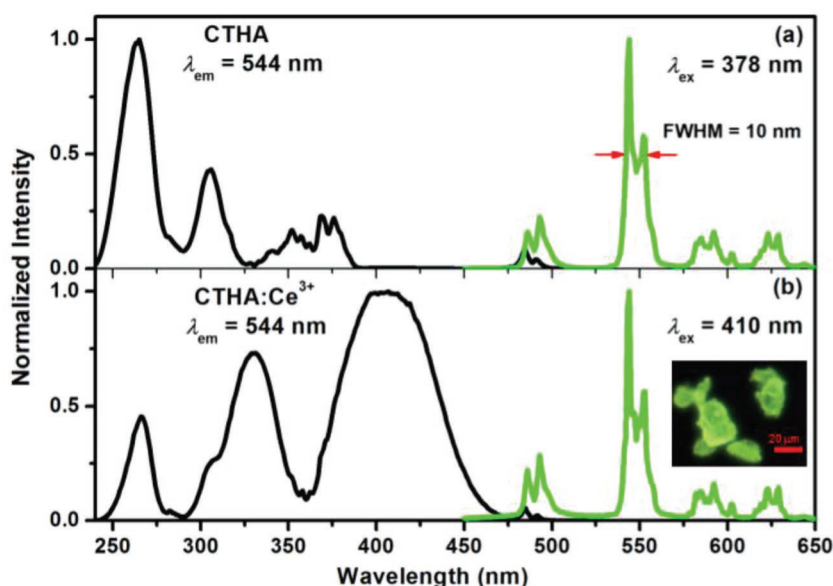
ADVANCED
SCIENCE NEWS
www.advancedsciencenews.com

ADVANCED
OPTICAL
MATERIALS
www.advopticalmat.de

Figure 2. a) The excitation and emission spectra of CTHA. b) The excitation and emission spectra of CTHA:Ce^{3+}. The inset shows the fluorescence microscopy image of CTHA:Ce^{3+} under 405 nm excitation.

HRTEM images (Figure 1c) exhibit clear lattice fringes with interplanar spacing of 2.765 and 4.416 Å corresponding to the (024) and (022) planes of CTHA, which further confirms that CTHA belongs to the garnet structure with the cubic system, as illustrated in Figure 1b. The energy-dispersive X-ray spectroscopy (EDS) was conducted to determine the chemical composition. The detected atomic ratios are approximate to the predicted composition (Table S3, Supporting Information). Besides, X-ray photoelectron spectroscopy (XPS) was performed to clarify the valence states of cerium and terbium of CTHA:0.05Ce^{3+}. As shown in Figure 1d,e, the high-resolution XPS spectra of Ce (3d) and Tb (3d) contain obvious peaks attributed to Ce^{3+} and Tb^{3+}, and no characteristic peaks of Tb^{4+}/Ce^{4+} can be found, indicating that Tb^{4+}/Ce^{4+} were fully reduced to Tb^{3+}/Ce^{3+} in CTHA under the atmosphere of 5%H$_2$/95%N$_2$.[12]

Figure 2a shows the excitation and emission spectra of CTHA. Upon 378 nm excitation of $^7F_6{\rightarrow}^5D_3$ transition, the emission spectrum of CTHA consists of a series of emission lines at 493, 544, 592, and 623 nm originating from the $^5D_4{\rightarrow}^7F_J$ (J = 6, 5, 4, and 3) transitions of Tb^{3+}, which is dominated by the green one. The excitation spectrum contains not only several excitation bands in the UV range (<380 nm) but also a weak excitation line at 485 nm. It is noteworthy that the full width at half maximum (FWHM) of the green emission is merely 10 nm, which is much smaller than that of all the previous green-emitting materials for display including YAG:Ce^{3+} (LuAG:Ce^{3+}) (>100 nm), β-Sialon:Eu^{2+} (RbLi(Li$_3$SiO$_4$)$_2$:Eu^{2+}) (>40 nm), and CdSe/ZnS (CsPbBr$_3$) quantum dots (QDs) (>20 nm).[13] If appropriate color filter is used, we can obtain extra pure green emission. In view of this unique feature, Tb^{3+}-activated materials were widely used for field emission display (Y$_2$SiO$_5$:Tb^{3+}) and electroluminescence display (ZnS:Tb^{3+}) before.[14] Nevertheless, those materials have no excitation band in the violet/blue range, thereby being completely excluded from LED/LD-based displays.

As Tb^{3+} increasingly occupies the Lu^{3+} site of CLHA, the emission intensity of Tb^{3+} $^5D_4$ level becomes higher, and shows a very small decrease when Lu^{3+} is fully replaced by Tb^{3+} (Figure S1, Supporting Information), indicating insignificant concentration quenching of Tb^{3+} emission in CTHA. However, the concentration quenching begins at the Tb^{3+} concentration of 10 mol% in other aluminate garnets.[15] This implies that the interaction between Tb^{3+} ions is relatively weak owing to the larger interionic distance of the nearby Tb^{3+}–Tb^{3+} pairs in CTHA (3.82 Å) as compared with YAG (3.67 Å). Because the oscillator strength of Tb^{3+} f–f transition (10^{-6}) is at least three orders of magnitude smaller than that of Ce^{3+} f–d transition (10^{-2}), the interaction between Ce^{3+} and Tb^{3+} will be sufficiently strong despite the weak interaction between Tb^{3+} ions, which is then effectively exploited to broaden and enhance the visible light excitation of Tb^{3+} in CTHA:Ce^{3+}.

The compounds of Ca$_2$Lu(Hf,Zr)$_2$Al$_3$O$_{12}$ can retain the garnet structure at atmospheric pressure when Lu^{3+} is fully replaced by Y^{3+} and Gd^{3+} with larger radii to form solid solutions,[16] and it is the same case for Tb^{3+} (i.e., CTHA). Considering that the cyan emission at 484 nm of CLHA:Ce^{3+} overlaps well with the $^7F_6{\rightarrow}^5D_4$ excitation line of Tb^{3+},[10] we introduced Ce^{3+} into CTHA to construct a Ce$^{3+}{\rightarrow}$Tb^{3+} ET system. In the excitation spectrum (Figure 2b) of CTHA:0.05Ce^{3+} with the optimized Ce^{3+} concentration of 5 mol% (Figure S2, Supporting Information), a new strong band appears around 410 nm spanning the whole violet spectral range from 380 to 450 nm, which is two orders of magnitude higher than those of Tb^{3+} f–f transitions and also much higher than the spin-allowed f–d excitation band of Tb^{3+} itself at 265 nm. The profile of this new band coincides well with that of CLHA:Ce^{3+},[10] indicating the occurrence of ET process from Ce^{3+} to Tb^{3+} as expected. These remarkable improvements can be attributed to the highly efficient ET process from Ce^{3+} to Tb^{3+} as well as the giant absorption coefficient of the 4f–5d allowed transition of Ce^{3+}. It can be seen from Figure 2b and the inset photograph that CTHA:0.05Ce^{3+} shows intense green emission originating from Tb^{3+}, while the cyan emission of Ce^{3+} is hardly seen, which means the ET efficiency is approaching 100%, benefiting from the concentrated Tb^{3+} in CTHA. Such high ET efficiency is also corroborated by the considerable shortening of the effective lifetime of Ce^{3+} emission after Lu^{3+} was fully replaced by Tb^{3+} in CLHA:Ce^{3+} (Figure S3, Supporting Information).

Under 410 nm excitation, the internal/external QEs of CTHA:0.05Ce^{3+} were determined to be 49.2%/32.3% (Figure S4, Supporting Information), which can be further improved by optimizing the preparation conditions and the compositions. Thanks to the limited concentration self-quenching of Tb^{3+}, CTHA:0.05Ce^{3+} shows just a small QE reduction as compared with CLHA:Ce^{3+} (50.3%),[10] indicating just negligible QE loss concomitant with the thorough emission tuning by the ET process from Ce^{3+} to Tb^{3+}. Unlike some of the previous works

where Tb^{3+} as well as Ce^{3+} replaces the divalent cations in the hosts,[17] there is no charge mismatch and only small difference of the ionic radii exists for the substitution of Lu^{3+} in CLHA, which ensure the heavy doping of Tb^{3+} and the complete energy transfer from Ce^{3+} to Tb^{3+}. Our results demonstrate that efficient visible light excitation is realizable for Tb^{3+}-activated materials via the strategy of sensitization. Besides, it should be noted that because of the large energy gap (about 0.5 eV) between the excitation of Ce^{3+} and the dominant green emission of Tb^{3+} (Figure S5, Supporting Information), the ubiquitous reabsorption for RGB phosphor blend can be attenuated significantly by using CTHA:Ce^{3+} instead of other Ce^{3+}/Eu^{2+}-activated green-emitting materials like β-Sialon:Eu^{2+}, and QDs like $CsPbBr_3$ and CdSe/ZnS, which is an obvious advantage of the strategy of sensitization to realize green (or red) emission.

Another key characteristic to be evaluated is the fluorescence thermal stability of CTHA:Ce^{3+} since heat generation is inevitable during LED/LD device operation. **Figure 3**a shows the integrated emission intensity of CTHA:0.05Ce^{3+} as a function of the temperature. The emission intensity gradually decreases with the temperature, and when the temperature is increased from 303 to 363 K and 423 K, the relative intensity drops to 92.5% and 72.6%, respectively. Owing to the smaller energy difference between the lowest 5d level of Ce^{3+} and $^5D_4$ level of Tb^{3+},

the back energy transfer from Tb^{3+} to Ce^{3+} will happen more easily with the assistance of heat, thus providing an additional nonradiative channel for $^5D_4$ level.[3c,d,4a,5b] Accordingly, the Tb^{3+} emission shows stronger thermal quenching in CTHA:Ce^{3+} than CTHA (94.1% at 423 K) (Figure S6, Supporting Information). Moreover, the FWHM as well as the peak wavelength of CTHA:0.05Ce^{3+} shows little change with the temperature below 423 K (Figure 3b), which is a universal character of Ln^{3+} f–f transitions resulting from the weak electron–phonon coupling between the 4f electrons and their surroundings. Hence, CTHA:Ce^{3+} possesses good fluorescence thermal stability.

To demonstrate that CTHA:Ce^{3+} can serve as a competitive candidate for display backlights, we fabricated the white LED device by combining a violet LED chip ($\lambda = 400$ nm) with the mixture of the green phosphor CTHA:0.05Ce^{3+}, the commercial red phosphor KSF:Mn^{4+}, and the commercial blue phosphor BAM:Eu^{2+}. The emission spectrum of the white LED at a forward bias current of 20 mA is shown in **Figure 4**a, and the inset presents the photograph of the lighted white LED. The color rendering index (R_a), the correlated color temperature (CCT), and the Commission Internationale de L'Eclairage (CIE) coordinates of the white light are 80.8, 6347 K, and (0.316, 0.330), respectively. The luminous efficiency (LE) was determined to be 31.2 lm W^{-1}, which is among the highest in the previously reported white LEDs based on near-UV (or violet) LEDs.[18] After passing through the traditional RGB color filters (CFs), the CIE coordinates of the RGB primary colors are (0.684, 0.313), (0.245, 0.605), and (0.134, 0.080) (Figure 4b, and see Figure S7 in the Supporting Information for the details). The white LED can attain a color gamut of 79% (coverage ratio) or 84% (area ratio) of National Television Standards Committee (NTSC) space in CIE 1931. Furthermore, the color gamut will reach up to 95% NTSC in coverage ratio and 104% NTSC in area ratio if a modified green CF is used to reduce the crosstalk.[18] Despite the broad emission of BAM:Eu^{2+}, the equivalent effect in color gamut has been achieved owing to the extra narrow green emission of CTHA:Ce^{3+}, as compared with that of white LED for display backlighting fabricated by β-Sialon:Eu^{2+} with peak wavelength at 540 nm,[7b,20] confirming that CTHA:Ce^{3+} is a promising alternative to the current green-emitting materials for wide-color-gamut display technology.

In summary, we have demonstrated that efficient visible light excitation of Tb^{3+} is achieved in terbium-concentrated garnet CTHA:Ce^{3+} owing to the high ET efficiency from Ce^{3+} to Tb^{3+} as well as limited concentration quenching among Tb^{3+} ions. CTHA:Ce^{3+} possesses ultra-narrow-band green emission with FWHM = 10 nm, which is even much narrower than that of $CsPbBr_3$ QDs. The prototype white LED device can attain a wide color gamut of 95% NTSC after passing
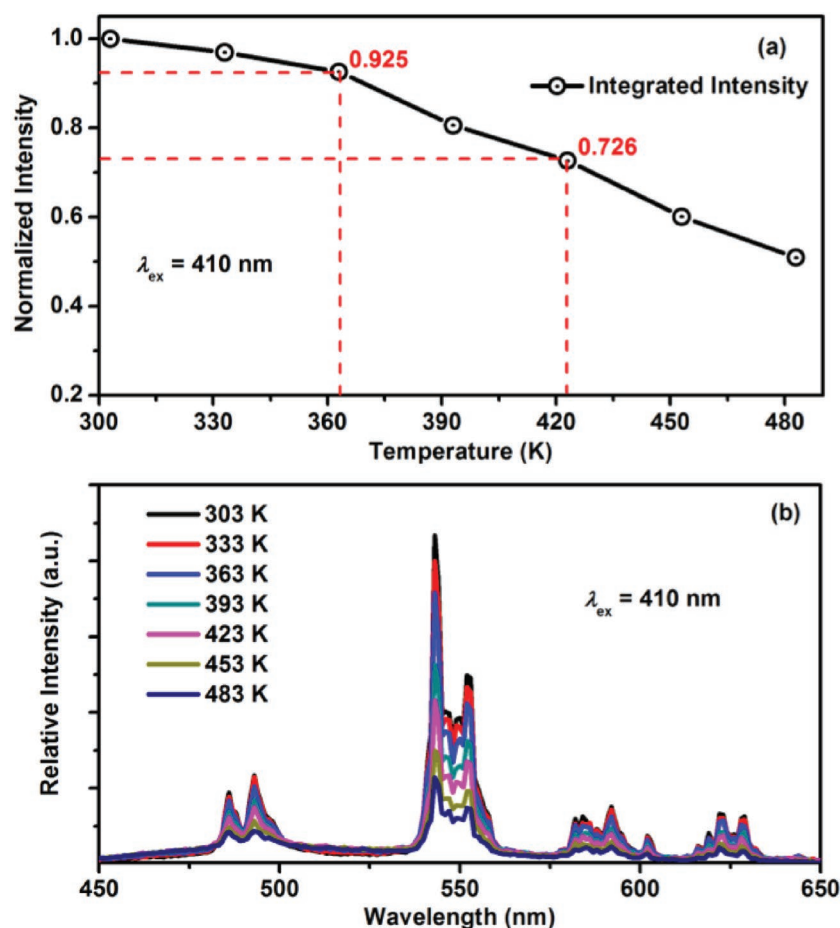

Figure 3. a) The integrated emission intensity of CTHA:0.05Ce^{3+} as a function of the temperature. b) Temperature dependent emission spectra of CTHA:0.05Ce^{3+} under 410 nm excitation.
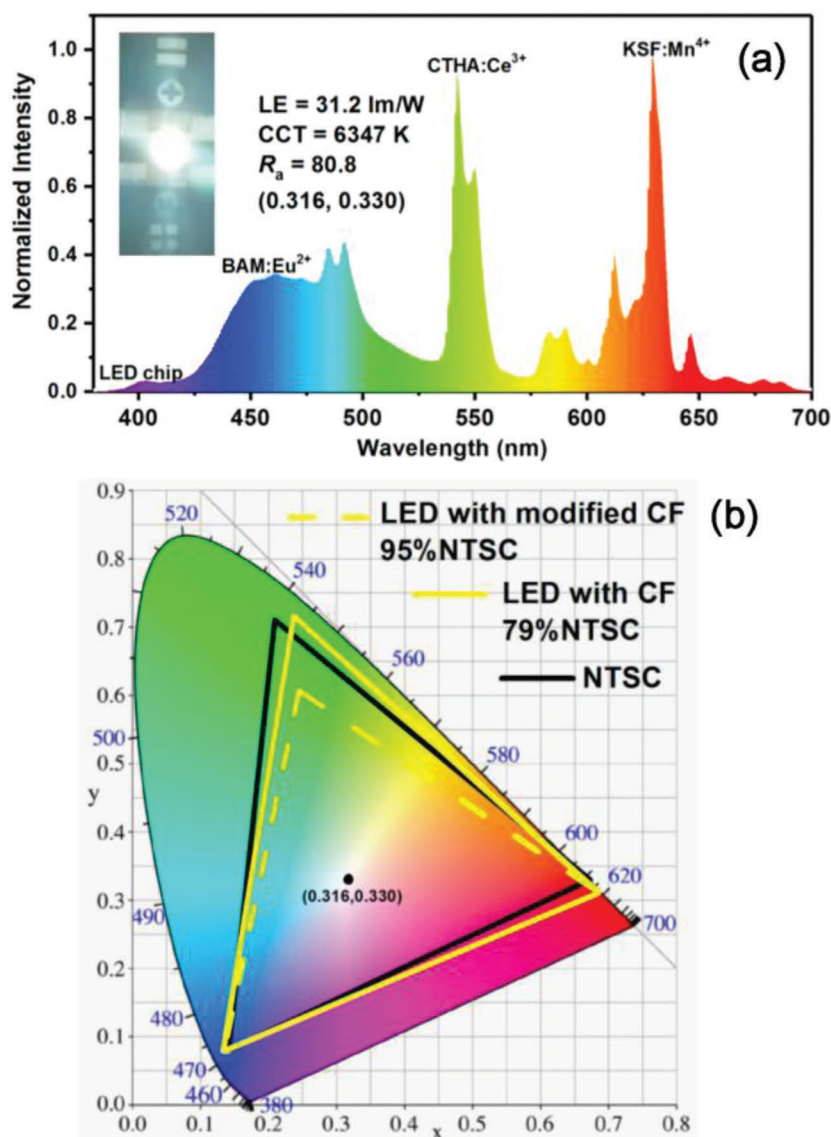
Figure 4. a) The emission spectrum of the fabricated white LED based on violet LED chip under a current of 20 mA. The inset shows a photo of the lighted white LED. b) CIE 1931 color coordinates of fabricated white LED, and color space of NTSC standard (black line) and white LED device (yellow line for the traditional CFs and yellow dashed line for the modified CFs).

through RGB CFs. Considering the possibility of being fabricated into translucent/transparent ceramics due to the optically isotropic properties of the cubic structure,[21] in addition to the facile synthesis and the high chemical and physical stabilities of garnet oxides, CTHA:Ce^{3+} can be used for high-power LED or even LD-based applications, and green laser is also expected in CTHA:Ce^{3+} crystal by using the violet LD as the excitation source.[3b]

Experimental Section

Materials and Preparation: The powder samples of Ce^{3+}-doped and undoped CTHA were synthesized via the traditional solid-state reaction. The stoichiometric amounts of CaCO$_3$ (99.99%), Lu$_2$O$_3$ (99.99%), Tb$_4$O$_7$ (99.99%), HfO$_2$ (99.99%), Al$_2$O$_3$ (99.9%), and CeO$_2$ (99.99%) were used

as the raw materials, and a small amount (3 wt%) of CaF$_2$ (99.99%) was added as the flux. These materials were weighed and thoroughly ground in an agate mortar for 30 min. The resulting mixtures were transferred into a lidded corundum crucible and then put into a tube furnace. The temperature was first stopped at 1000 °C for 2 h to decompose the carbonate, and then raised to 1540 °C and maintained for 6 h to obtain the expected crystalline phase. In the whole sintering process, a reducing atmosphere of 5%H$_2$/95%N$_2$ with a constant flow was used. Finally, the synthesized product was reground into fine powders for characterizations.

Characterization: Powder XRD patterns of all samples were obtained on a Bruker D8 Focus diffractometer (Cu Kα radiation ($\lambda = 1.54056$ Å, 40 kV and 40 mA), in the 2θ range from 10° to 75°. The scanning rate was set at 1 s per step with a step size of 0.02°. The Rietveld refinement was conducted by using the FullProf program.[22] HRTEM images were measured on a transmission electron microscope (JEM-2100F, JEOL) at an operating voltage of 200 kV. XPS spectra were collected by using a Thermo Scientific Escalab 250Xi spectrometer with an Al Kα radiation as the excitation source. The elementary composition was analyzed by an energy-dispersive spectrometer (EDS) (INCA Energy Coater, Oxford Instruments) coupled to a field emission scanning electron microscopy (Ultra-55, Carl Zeiss). Excitation and emission spectra, the decay curves, as well as the temperature-dependent spectra were measured on FLS920P spectrometer (Edinburgh Instruments), where a picosecond pulsed diode laser ($\lambda_{em} = 374.6$ nm, pulse width 81.3 ps, Edinburgh Instruments EPL-375) was used as the excitation source for the decay curves, and the temperature was controlled by a high-temperature fluorescence test device (TAP-02, Orient KOJI). Fluorescence microscope image was recorded on the fluorescence microscope (BX53M, OLYMPUS) in the dark-field mode using a 405 nm lamp as the excitation source. The internal/external quantum efficiencies were measured with an absolute photoluminescence quantum yield measurement system (Quantaurus-QY Plus C13534-12, Hamamatsu Photonics). The electroluminescence spectra, R_a, CCT, and luminous efficiency of the fabricated white LEDs were obtained on an integrated test system (LHS-1000, EVERFINE) including photoelectric characteristic testing system, high accuracy array spectrophotometer (HAAS-2000), dc stabilized current power supply, and a rotating integral ball. It should be noted that the violet LED chips (405 nm) were produced by Guangsheng Semiconductor Technology Co., Ltd. (chip size is 1.143 × 1.143 mm and photoelectric conversion efficiency is 43%).

Supporting Information

Supporting Information is available from the Wiley Online Library or from the author.

Acknowledgements

Conflict of Interest

The authors declare no conflict of interest.

Keywords

[1] a) P. Pust, P. J. Schmidt, W. Schnick, *Nat. Mater.* **2015**, *14*, 454; b) E. H. Penilla, L. F. Devia-Cruz, M. A. Duarte, C. L. Hardin, Y. Kodera, J. E. Garay, *Light: Sci. Appl.* **2018**, *7*, 33; c) D. Zhou, D. Liu, G. Pan, X. Chen, D. Li, W. Xu, X. Bai, H. Song, *Adv. Mater.* **2017**, *29*, 1704149; d) S. Wen, J. Zhou, K. Zheng, A. Bednarkiewicz, X. Liu, D. Jin, *Nat. Commun.* **2018**, *9*, 2415; e) H. Dong, S. R. Du, X. Y. Zheng, G. M. Lyu, L. D. Sun, L. D. Li, P. Z. Zhang, C. Zhang, C. H. Yan, *Chem. Rev.* **2015**, *115*, 10725.

[2] a) G. Liu, J. Bernard, *Spectroscopic Properties of Rare Earths in Optical Materials*, Springer Series in Materials Science, Vol. *83*, Springer, Berlin **2006**, pp. 95–129; b) D. C. Yu, R. Martin-Rodriguez, Q. Y. Zhang, A. Meijerink, F. T Rabouw, *Light: Sci. Appl.* **2015**, *4*, e344; c) J. C. Zhang, C. Pan, Y. F. Zhu, L. Z. Zhao, H. W. He, X. Liu, J. Qiu, *Adv. Mater.* **2018**, *30*, 1804644.

[3] a) K. Kömpe, H. Borchert, J. Storz, A. Lobo, S. Adam, T. Möller, M. Haase, *Angew. Chem., Int. Ed.* **2003**, *42*, 5513; b) P. W. Metz, D. T. Marzahl, A. Majid, C. Kränkel, G. Huber, *Laser Photonics Rev.* **2016**, *10*, 335; c) G. Bao, K. L. Wong, D. Jin, P. A. Tanner, *Light: Sci. Appl.* **2018**, *7*, 96; d) Y. Cui, H. Xu, Y. Yue, Z. Guo, J. Yu, Z. Chen, J. Gao, Y. Yang, G. Qian, B. Chen, *J. Am. Chem. Soc.* **2012**, *134*, 3979.

[4] a) S. Omagari, T. Nakanishi, Y. Kitagawa, T. Seki, K. Fushimi, H. Ito, A. Meijerink, Y. Hasegawa, *Sci. Rep.* **2016**, *6*, 37008; b) C. C. Lin, W. T. Chen, C. I. Chu, K. W. Huang, C. W. Yeh, B. M. Cheng, R. S. Liu, *Light: Sci. Appl.* **2016**, *5*, e16066; c) J. McKittrick, M. E. Hannah, A. Piquette, J. K. Han, J. I. Choi, M. Anc, M. Galvez, H. Lugauer, J. B. Talbot, K. C. Mishra, *ECS J. Solid State Sci. Technol.* **2013**, *2*, R3119; d) P. P. Dai, C. Li, X. T. Zhang, J. Xu, X. Chen, X. L. Wang, X. Wang, Y. C. Liu, *Light: Sci. Appl.* **2016**, *5*, e16024.

[5] a) K. Li, M. Shang, H. Lian, J. Lin, *J. Mater. Chem. C* **2016**, *4*, 5507; b) E. Deiters, B. Song, A. S. Chauvin, C. D. Vandevyver, F. Gumy, J. C. G. Bünzli, *Chem. - Eur. J.* **2009**, *15*, 885; c) W. Shao, C. K. Lim, Q. Li, M. T. Swihart, P. N. Prasad, *Nano Lett.* **2018**, *18*, 4922;

d) B. Chen, D. Peng, X. Chen, X. Qiao, X. Fan, F. Wang, *Angew. Chem., Int. Ed.* **2015**. *54*, 12788; *Angew. Chem.* **2015**, *127*, 12979.

[6] a) D. Wu, W. Xiao, L. Zhang, X. Zhang, Z. Hao, G. H. Pan, Y. Luo, J. Zhang, *J. Mater. Chem. C* **2017**, *5*, 11910; b) Y. Xiao, Z. Hao, L. Zhang, W. Xiao, D. Wu, X. Zhang, G. H. Pan, Y. Luo, J. Zhang, *Inorg. Chem.* **2017**, *56*, 4538; c) J. L. Sommerdijk, J. V. D. D. De Bye, P. Verberne, *J. Lumin.* **1976**, *14*, 91.

[7] a) Y. T. Tsai, C. Y. Chiang, W. Zhou, J. F. Lee, H. S. Sheu, R. S. Liu, *J. Am. Chem. Soc.* **2015**, *137*, 8936; b) S. Li, L. Wang, D. Tang, Y. Cho, X. Liu, X. Zhou, L. Lu, L. Zhang, T. Takeda, N. Hirosaki, R. J. Xie, *Chem. Mater.* **2018**, *30*, 494.

[8] a) M. Zhang, Y. Liang, R. Tang, D. Yu, M. Tong, Q. Wang, Y. Zhu, X. Wu, G. Li, *RSC Adv.* **2014**, *4*, 40626; b) R. Sato, S. Takeshita, T. Isobe, T. Sawayama, S. Niikura, *ECS J. Solid State Sci. Technol.* **2012**, *1*, R163.

[9] a) P. Dorenbos, *J. Phys.: Condens. Matter* **2003**, *15*, 4797; b) L. Wang, R. J. Xie, T. Suehiro, T. Takeda, N. Hirosaki, *Chem. Rev.* **2018**, *118*, 1951.

[10] X. Wang, Z. Zhao, Q. Wu, Y. Li, Y. Wang, *J. Mater. Chem. C* **2016**, *4*, 11396.

[11] R. D. Shannon, *Acta Crystallogr. A* **1976**, *32*, 751.

[12] a) P. Luches, F. Pagliuca, S. Valeri, *Phys. Chem. Chem. Phys.* **2014**, *16*, 18848; b) S. Zhang, Y. Li, Y. Lv, L. Fan, Y. Hu, M. He, *Chem. Eng. J.* **2017**, *322*, 314.

[13] a) H. W. Chen, J. H. Lee, B. Y. Lin, S. Chen, S. T. Wu, *Light: Sci. Appl.* **2018**, *7*, 17168; b) M. Zhao, H. Liao, L. Ning, Q. Zhang, Q. Liu, Z. Xia, *Adv. Mater.* **2018**, *30*, 1802489; c) S. Abe, J. J. Joos, L. I. Martin, Z. Hens, P. F. Smet, *Light: Sci. Appl.* **2017**, *6*, e16271; d) X. Li, Y. Wu, S. Zhang, B. Cai, Y. Gu, J. Song, H. Zeng, *Adv. Funct. Mater.* **2016**, *26*, 2435.

[14] T. Jüstel, H. Nikol, C. Ronda, *Angew. Chem., Int. Ed.* **1998**, *37*, 3084; *Angew. Chem.* **1998**, *110*, 3250.

[15] a) X. Teng, J. Li, G. Duan, Z. Liu, *J. Lumin.* **2016**, *179*, 165; b) G. Xia, S. Zhou, J. Zhang, S. Wang, J. Xu, *J. Alloys Compd.* **2006**, *421*, 294.

[16] a) X. Gong, J. Huang, Y. Chen, Y. Lin, Z. Luo, Y. Huang, *Inorg. Chem.* **2014**, *53*, 6607; b) L. Zhang, S. Zhang, Z. Hao, X. Zhang, G. H. Pan, Y. Luo, H. Wu, J. Zhang, *J. Mater. Chem. C* **2018**, *6*, 4967.

[17] a) Z. Xia, R. S. Liu, *J. Phys. Chem. C* **2012**, *116*, 15604; b) G. Li, Y. Wang, W. Zeng, W. Chen, S. Han, H. Guo, Y. Li, *J. Mater. Chem. C* **2016**, *4*, 3304; c) W. Lü, N. Guo, Y. Jia, Q. Zhao, W. Lv, M. Jiao, B. Shao, H. You, *Inorg. Chem.* **2013**, *52*, 3007.

[18] a) Y. H. Kim, P. Arunkumar, B. Y. Kim, S. Unithrattil, E. Kim, S. H. Moon, J. Y. Hyun, K. H. Kim, D. Lee, J. S. Lee, W. B. Im, *Nat. Mater.* **2017**, *16*, 543; b) Z. Wang, J. Ha, Y. H. Kim, W. B. Im, J. McKittrick, S. P. Ong, *Joule* **2018**, *2*, 914; c) Y. Liu, J. Silver, R. J. Xie, J. Zhang, H. Xu, H. Shao, J. Jiang, H. Jiang, *J. Mater. Chem. C* **2017**, *5*, 12365.

[19] a) H. W. Chen, R. D. Zhu, J. He, W. Duan, W. Hu, Y. Q. Lu, M. C. Li, S. L. Lee, Y. J. Dong, S. T. Wu, *Light: Sci. Appl.* **2017**, *6*, e17043; b) R. Zhu, Z. Luo, H. Chen, Y. Dong, S. T. Wu, *Opt. Express* **2015**, *23*, 23680.

[20] H. Liao, M. Zhao, M. S. Molokeev, Q. Liu, Z. Xia, *Angew. Chem., Int. Ed.* **2018**, *57*, 11728; *Angew. Chem.* **2018**, *130*, 11902.

[21] A. Goldstein, A. Krell, *J. Am. Ceram. Soc.* **2016**, *99*, 3173.

[22] J. Rodríguez-Carvajal, in *Abstracts of the Satellite Meeting on Powder Diffraction of the 15th Int. Congress of the IUCr*, Toulouse, France **1990**, p. 127.